Modelling of high temperature flow stress of VN and Nb-Ti microalloyed steels during hot compressive deformation

Chalimba S.A.J., Mostert R.J., Stumpf W.E., Siyasiya C.W., Banks K.M.
Department of Materials Science and Metallurgical Engineering, University of Pretoria, Hatfield, Pretoria, Republic of South Africa
Corresponding author: Tel: +27 606 033 216
Email: stephenchalimba@yahoo.com

Key words: modelling, flow stress, dynamic transformation, dynamic recrystallization, hot rolling

Abstract
A simple mathematical model has been developed which describes the flow curve behaviour up to the peak true stress or a true strain of 0.6 in unstable austenite. The hot working behaviour was analysed by compression tests over a temperature range of 750 – 1000 ^{o}C and at strain rates of 0.1 – 50 s^{-1}. The constitutive behaviour focused on the interaction between work hardening and dynamic softening attributed to recovery, recrystallization and dynamic austenite to ferrite transformation. This model extends the application of the well-established Estrin and Mecking (EM) work-hardening model in the unstable austenite region. The work hardening is countered by softening kinetics, represented in this model by JMAK type expressions for both dynamic transformation and recrystallization. The predicted results correlate well with experimental results in VN and Nb-Ti microalloyed steels.

1.0 Introduction

A successful design of an industrial hot working process requires fundamental knowledge of microstructural evolution whilst defining the dependence of the flow curve on deformation variables (i.e. strain, strain rate and temperature) [1]. Most constitutive models describing the hot rolling behaviour of steels are developed for the stable austenite temperature range (between 950-1150 ^{o}C) and at quasi-static strain rates of 0.001-0.1 s^{-1} where steady state conditions are applicable, and recrystallization is the only favourable or dominant softening mechanism [1, 2, 3]. In the final passes in the finishing mill, however, hot rolling may be done in the unstable austenite and intercritical phase region where complex relationships between flow strength and various mechanisms such as work-hardening, recrystallization, precipitation, and transformation exist. This condition covers width (edges which cool faster) and length of thin hot rolled strip gauges.

Various flow stress models applied in industry were reviewed which included the Arrhenius equation, Misaka (including the Misaka reloaded model [4]), Cingara, Solhjoo and Shida [5] models to assess their applicability in the unstable austenite region, see Figure 1. Experimental Mean Flow Stress (MFS) data, obtained for both VN and Nb-Ti microalloyed steels, was compared to the predicted MFS determined using the above-mentioned models. The experimental flow stress data and predictions from mathematical models were converted to MFS for comparison purposes with MFS predictions from the empirical models. The Misaka and modified Misaka models predicted relatively very low MFS levels

than the experimental MFS curve due to the exaggeration of the influence of dynamic recrystallization (DRX). The Shida and Misaka reloaded had the initial part of the which predicted higher stress levels than experimental flow stress and predicted MFS lower experimental values after a strain between 0.2 and 0.3. This was attributable to the fact that all the models considered do not account for effects of dynamic transformation (DT) which in most cases precedes DRX. The Cingara equation predicted higher MFS values to the MFS levels obtained from experimentation since DRX and DT are not considered.

It can be observed that the models applicable in the low temperature austenite are mostly empirical with weak mathematical relationships, which do not directly account for dynamic softening due to both transformation and recrystallization. Another challenge faced during rolling in the unstable austenite region is mill load fluctuations which may lead to mill instability and poor gauge control. On the other hand, the quest for process optimization and product improvement through improved physical and mechanical properties (i.e. grain refinement which improves strength ratio, ductility and toughness) in as-rolled products has led to controlled rolling below T_{nr} despite the existing knowledge gaps, especially in VN steels.

The aim of this work, therefore, is to introduce a simple but effective flow stress model applicable to the unstable austenite phase region in hot strip rolling of VN and Nb-Ti microalloyed steels. The model presented can easily be incorporated into Finite Element codes for online process control in hot strip mills.

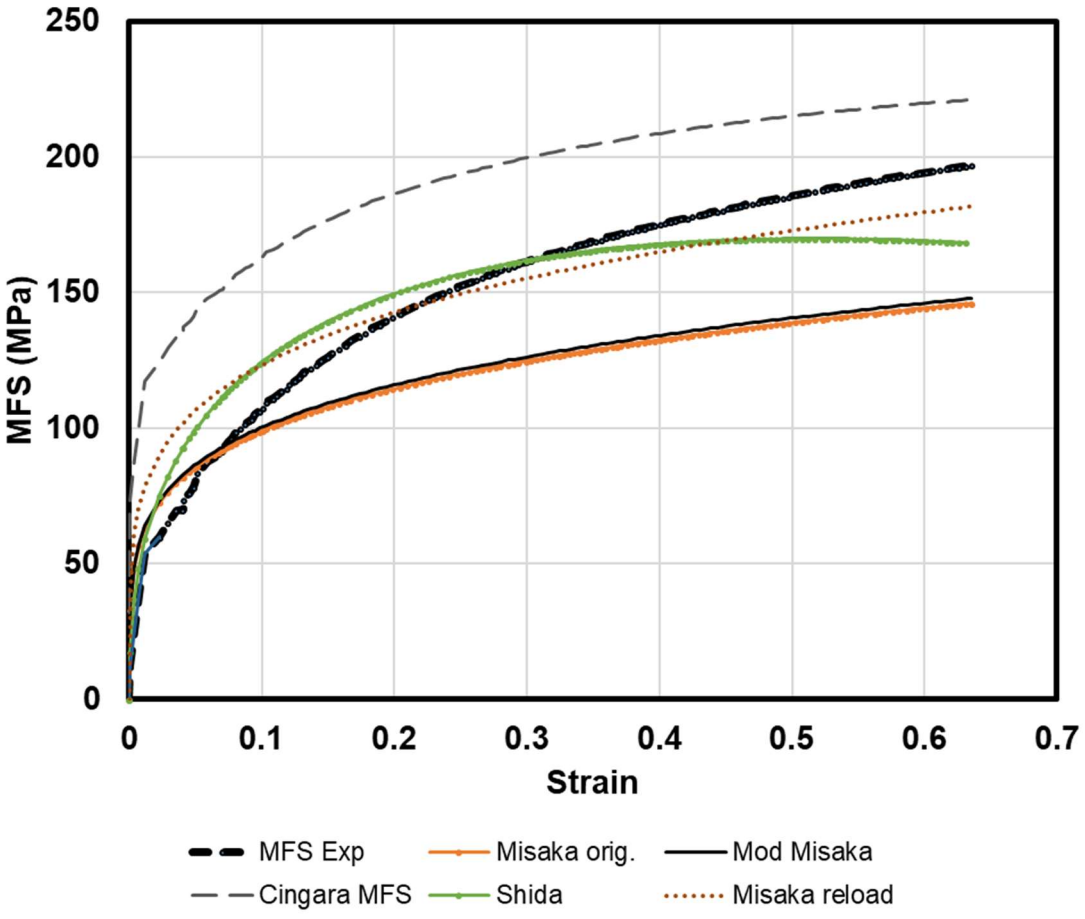

Figure 1 – Comparison of various flow stress models in VN microalloyed steels

2.0 Experimental procedure

2.1 Composition and sample preparation

VN and Nb-Ti microalloyed steels with chemical compositions given in Table I, were studied. For the VN steel, a vacuum induction melted ingot was hot rolled to 13 mm diameter bar, whilst the Nb-Ti steel specimens were wire cut from an as-cast industrial slab. Forty eight (48) axisymmetric hot compression specimens were wire cut to a height of 15 mm and diameter of 10 mm whereas dilatometric samples were machined to a height of 10 mm and diameter of 5 mm. An aspect ratio of 1.5 was maintained on specimens to minimize sample geometry influence on test results.

Table I – Chemical composition (mass-%) for the steels investigated

Steel	Element								
	C	Mn	Si	Al	Nb	Ti	V	N	Fe
VN	0.06	1.69	0.29	0.049	0.0015	Trace	0.062	0.0097	Bal.
Nb-Ti	0.09	0.88	0.20	0.043	0.025	0.017	0	0.0088	Bal.

Note: Combustiometric chemical analysis was used in the determination of C and N

2.2 Mechanical testing

Gleeble™ 1500 and Gleeble™ 3500 series thermomechanical simulators fitted with tungsten carbide (WC) anvils were used for isothermal uniaxial axisymmetric compression tests. The platens were lubricated either with tantalum foil or graphite and nickel paste. The specimens were deformed in accordance with the schematic schedule shown in Figure 2. Two passes were done with the first roughing deformation pass included to eliminate the effects of prior microstructural history, and ensure that all specimens experience equivalent hot deformation conditions and are at same initial state of microalloying elements. The microstructures after the roughing pass are provided in Figure 3. An austenitisation temperature of 1200 °C was applied in all tests based on typical industrial practice and dissolution temperatures of both V(C,N) – 854 °C and Nb(C,N) – 1092 °C determined from ThermoCalc® 4.1 property diagrams using the TCFE7 database. The criteria outlined in Ref [7,8,9] was used to validate the hot compression tests after upsetting. The testing criteria included the following parameters: the aspect ratio, and barrelling, height, ovality and circularity coefficients. Microstructure analysis was performed at the centre of an axially-sectioned plane of the deformed specimens.

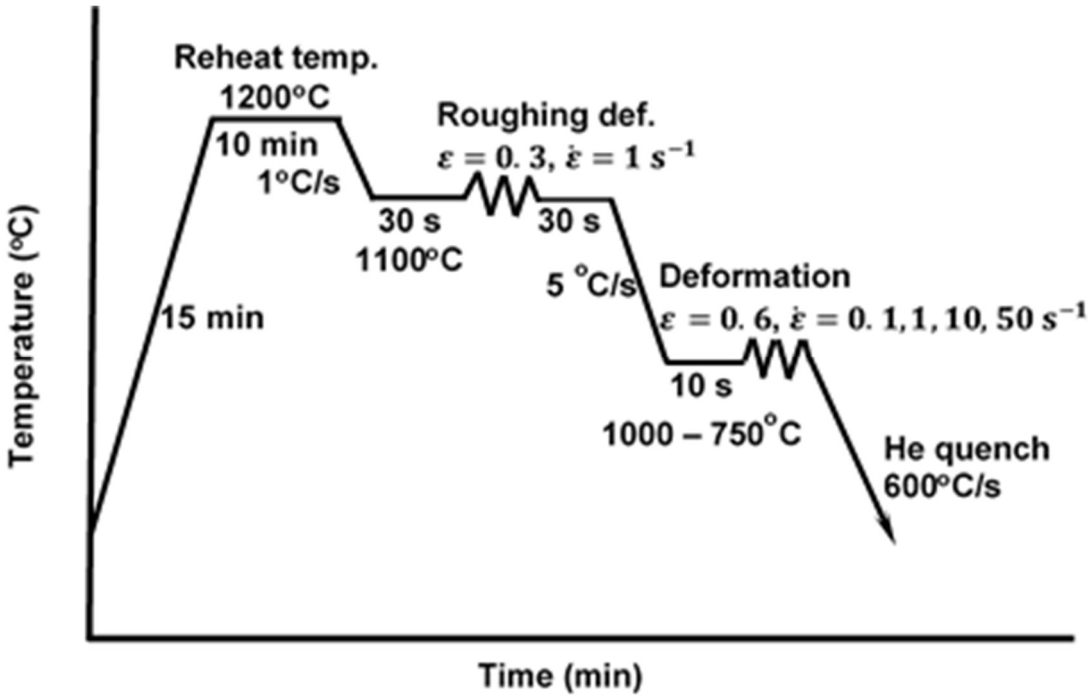

Figure 2 – Schematic representation of deformation test schedules. True strain and strain rate are represented as ε and $\dot{\varepsilon}$, respectively.

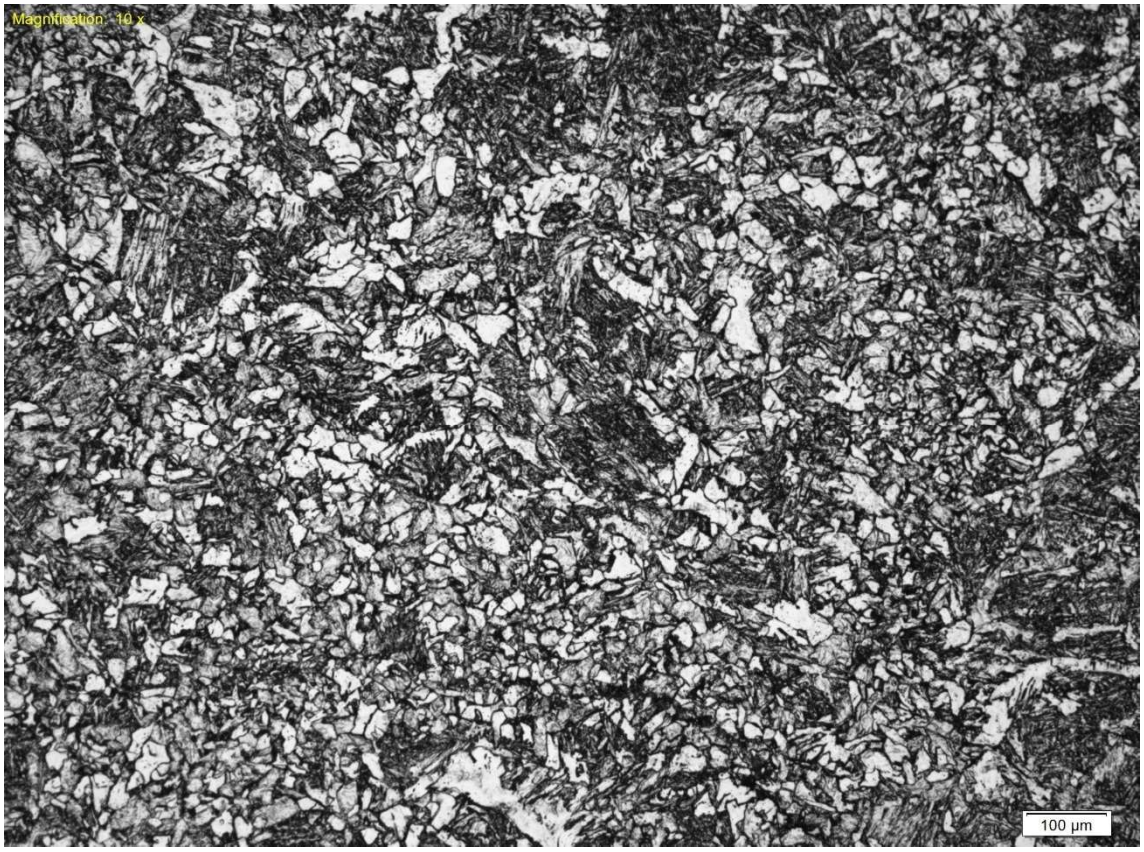

a)

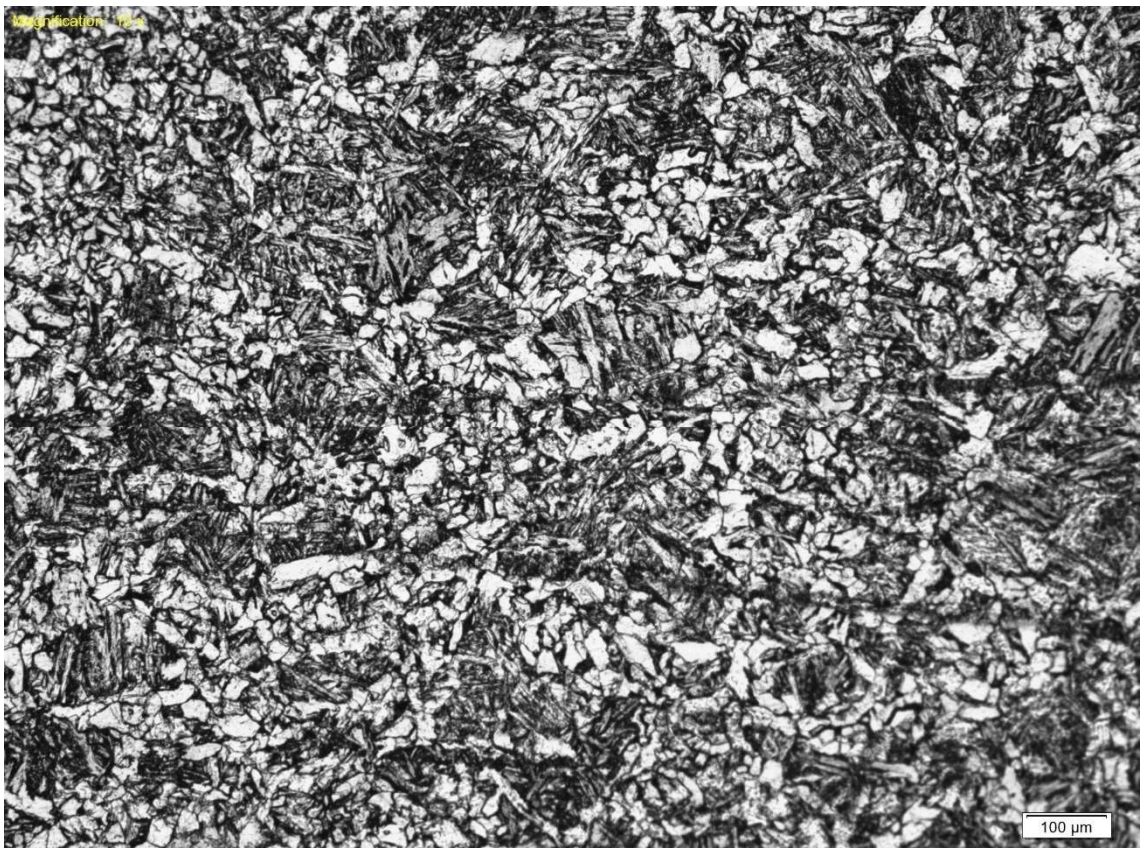

b)

Figure 3 – Microstructures after the roughing pass for a) VN steel and b) Nb-Ti steel at 1100°C

An inductive-heating Bähr™805 AD quenching and deformation dilatometer was used to determine the continuous cooling critical transformation temperatures. The Ar_3 temperatures after the first pass in Figure 2 was determined to be 843 °C for the VN steel and 818 °C for the Nb-Ti steel at a cooling rate of 5 °C/s, see Ref. [10]. The dilatation curves were used to determine the ferrite volume fractions at the start of the final deformation step [10].

2.3 Post-deformation flow stress data processing

A detailed flow curve analysis included the use of central differences, whilst graphical methods involved polynomial fitting and regression analysis of flow stress-strain data. Care was taken not to mask any metallurgical phenomena on the flow data. The curves were fitted to the macroscopic work-hardening flow curve using the yield stress $\sigma_{0.02}$ which was determined using the 2% offset strain method [11]. The plastic flow curve segment was fitted and smoothed with a 6th order polynomial using the Excel™ software. The percentage error attributable to the error inherent in temperature, load measurement, lubrication breakdown and non-uniform flow was expected to be below 4% [12].

The onset of DT and DRX, as defined by the double differentiation method, requires that the local stored energy in the deformed material attains a maximum critical value while the rate of dissipation must decrease to a minimum value [13]. This condition is expressed mathematically as:

$$\frac{\partial}{\partial \varepsilon}\left(-\frac{\partial \ln \theta}{\partial \varepsilon}\right) = 0$$

The critical strains for initiation of dynamic transformation ($\varepsilon_{c\,DT}$) and DRX ($\varepsilon_{c\,DRX}$) during deformation were determined by inflections on the $\ln\theta$–ε plots, where θ is the work-hardening rate. The critical strains are given as the single minima in $\partial \ln\theta/\partial\varepsilon$ versus ε plots, representing $\varepsilon_{c\,DT}$ and $\varepsilon_{c\,DRX}$ at low and high temperatures respectively or $\varepsilon_{c\,DT}$ followed by $\varepsilon_{c\,DRX}$ for double minima plots at intermediate temperatures. The rate of progression of DT and DRX was also assessed from the slope of $d\ln\theta/d\varepsilon$ versus ε plots. This method enabled the determination of critical strains by fitting sixth-order polynomials compared to the commonly used θ versus σ curves that require fitting of ninth- or higher order polynomials [14, 15]. The method was also considered more appropriate for determination of critical strains considering its higher correlation coefficients than θ versus σ plots [16, 13].

An assessment of theoretical modelling of the flow behaviour was performed up to the saturation stress (σ_{sat}) considering only work hardening and DRV. The modified work-hardening model utilised the linearity of $\sigma\theta - \sigma^2$ plots to define the DRV (including recovery factor), DT and DRX regimes. The deviation from linearity signified the critical stress, σ_c.

3.0 Results

3.1 The modified DRV work-hardening model

In the unstable austenite temperature region, the following restoration mechanisms compete: dynamic recovery, dynamic transformation and dynamic recrystallization. Plots of $\sigma\theta - \sigma^2$ were used to study work-hardening behaviour [6]. When DRV is the only softening mechanism (i.e. below the critical strain for both DT and DRX or theoretical DRV-only curve after the critical strain), the flow behaviour obeyed the following modified DRV work-hardening model for the inter-mode region [6]:

$$\boldsymbol{\sigma_{DRV}} = \left[\boldsymbol{\sigma_{sat}^2} - \left(\boldsymbol{\sigma_{sat}^2} - \boldsymbol{\sigma_0^2}\right)\mathbf{exp}\left(-\left(\frac{r}{s_r}\right)(\boldsymbol{\varepsilon} - \boldsymbol{\varepsilon_0})\right)\right]^{\mathbf{1/2}} \qquad \text{Equation 1}$$

where s_r is the softening rate, r is the recovery rate and (r/s_r) is the curvature factor.

The curvature factor which describes the predicted or hypothetical work-hardening stress curve when work-hardening is counteracted by DRV, DT and DRX, was given by the experimentally determined parameter $\frac{r}{s_r} \sim 1.2$ for the VN steel while $\frac{r}{s_r} \sim$ 1.5 for the Nb-Ti steel [6].

At low temperatures, where DT is the only softening mechanism and at high temperatures where DRX is dominant, the work-hardening true stress-strain curve obeys the following redefined original EM model [17]:

$$\boldsymbol{\sigma_{DRV} = \left[\sigma_{sat}^2 - \left(\sigma_{sat}^2 - \sigma_0^2\right) \exp\left(-s_r(\varepsilon - \varepsilon_0)\right)\right]^{1/2}}$$ Equation 2

For temperatures where DT-only or DRX-only is dominant, the softening rate $\boldsymbol{s_r}$ was found to be comparable, i.e. ~5.4 for both VN and Nb-Ti steels.

It should be noted that with an increase in strain rate, as typically experienced in the hot strip rolling mill, deformation will mostly be in the unstable austenite region, i.e. Equation 1 then applies.

3.2 Determination of material constants

The application of the Arrhenius kinetic equations originally developed by Garofalo for creep analysis [18, 19] during hot working as proposed by Sellars and Tegart [20], has been employed extensively in the literature in determination of the activation energy. The Power law expression (Equation 3) is suitable for low stresses since linearity is established at low stress levels ($\alpha\sigma < 0.8$) while linearity for the Exponential law (Equation 4) is achieved at high stress levels ($\alpha\sigma > 1.2$). The hyperbolic sinh law (Equation 5) is applicable at all stress levels.

$$Z = f(\sigma) = A'\sigma^n$$ Equation 3

$$Z = f(\sigma) = A'' \exp(\beta\sigma)$$ Equation 4

$$Z = f(\sigma) = A[\sinh(\alpha\sigma)]^n$$ Equation 5

The material constants: A, stress sensitivity factor β, stress multiplier α and stress exponent n, were derived for the power law, exponential law and hyperbolic sinh law, respectively, see Figure 4.

The activation energy for hot working Q_{HW}, used in this study were determined using the Arrhenius expressions and plots given in Figure 5. The activation energy Q_{HW} is evaluated to be ~156 kJ/mol for the Nb-Ti and ~128 kJ/mol for the VN steels. The flow stress dependency on temperature and strain rate (i.e. thermal and strain rate work-hardening) was expressed through the temperature compensated strain rate or the Zener–Hollomon parameter (Z), see Table IV. The Zener-Hollomon parameter is mathematically expressed as:

$$Z = \dot{\varepsilon} \exp\left(\frac{Q_{HW}}{RT}\right)$$ Equation 6

where Q_{HW} is the hot working activation energy, R is the gas constant and T is the absolute temperature.

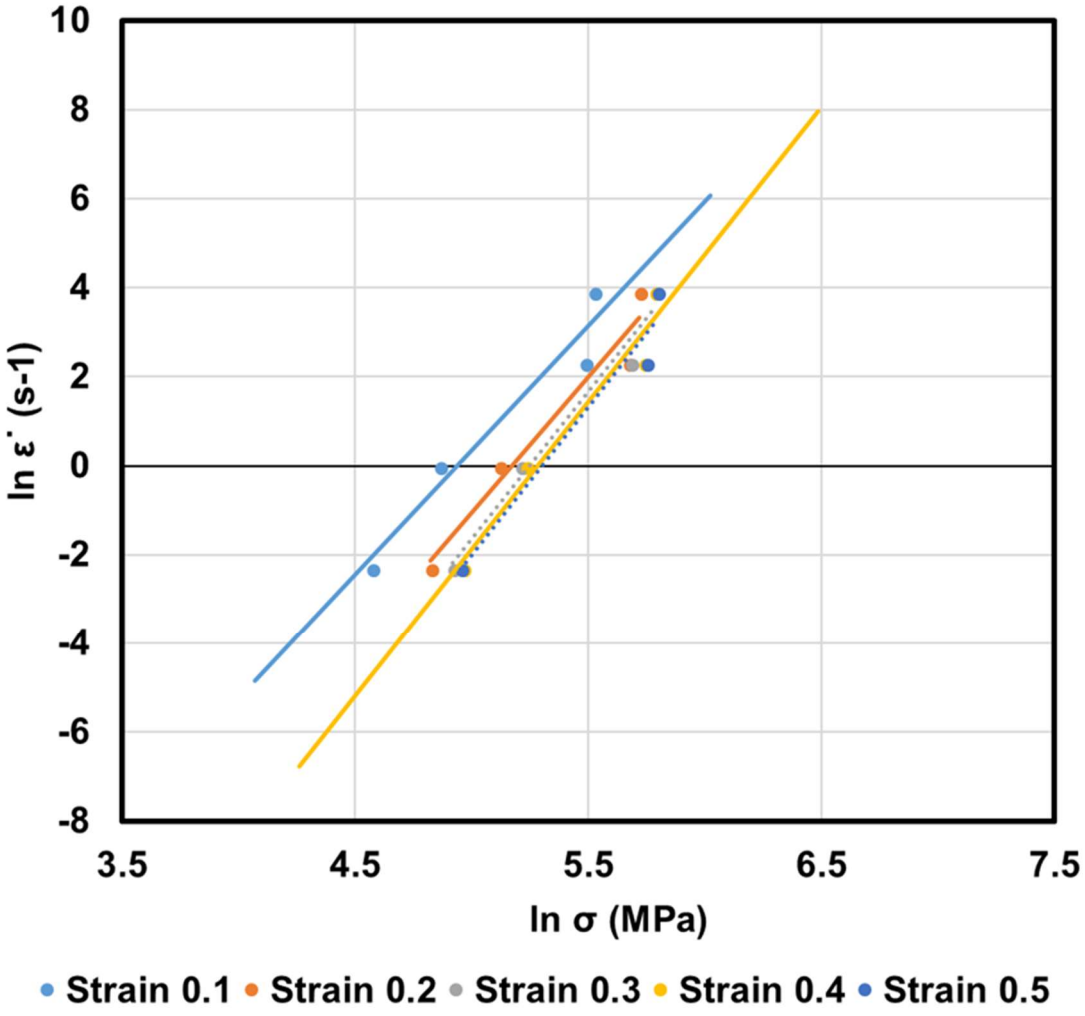

Temperature (°C)	850	850	850	850	850
Strain	0.5	0.4	0.3	0.2	0.1
n'	6.6635	6.6112	6.6034	6.083	5.5954
Y axis intercept	-35.33	-34.91	-34.67	-31.45	-27.62
R^2	0.9597	0.9566	0.9771	0.955	0.9439

a)

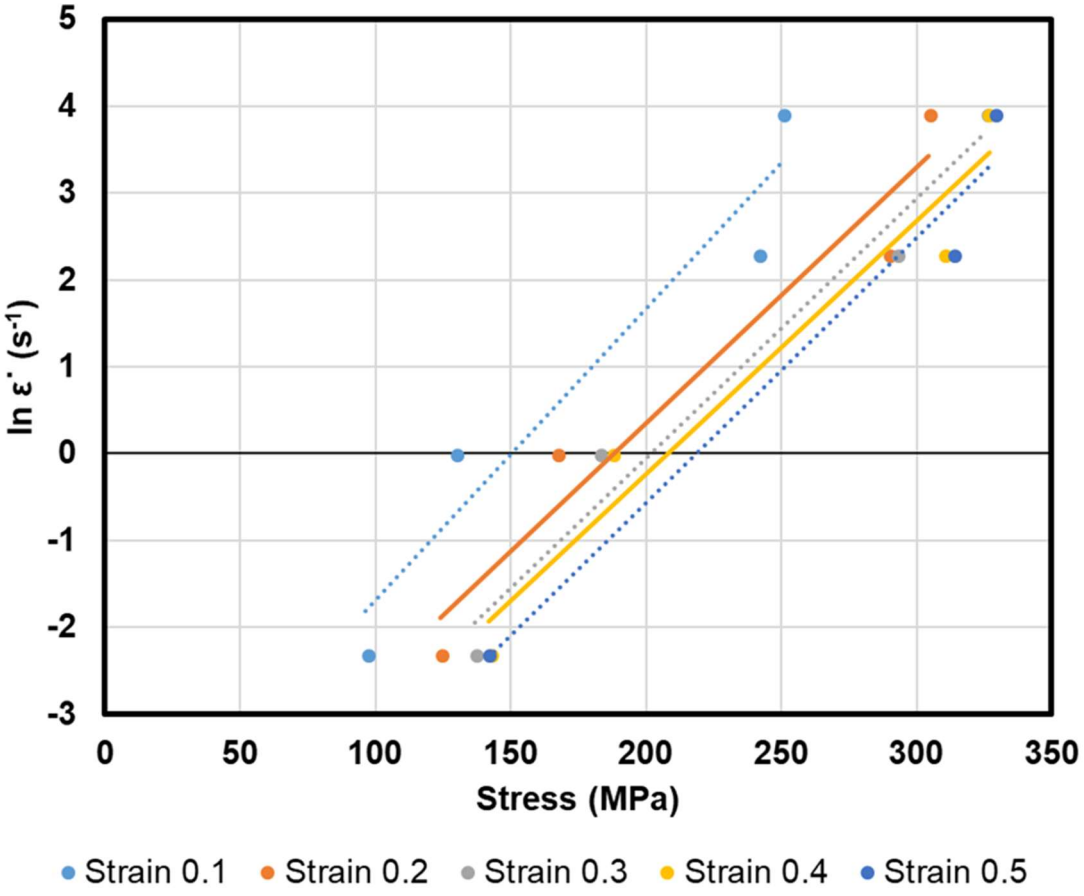

Temperature (°C)	850	850	850	850	850
Strain	0.5	0.4	0.3	0.2	0.1
β	0.0305	0.0291	0.0299	0.0265	0.0334
Y axis intercept	-6.662	-6.053	-6.039	-5.542	-5.025
R^2	0.9683	0.946	0.9698	0.9428	0.9263

b)

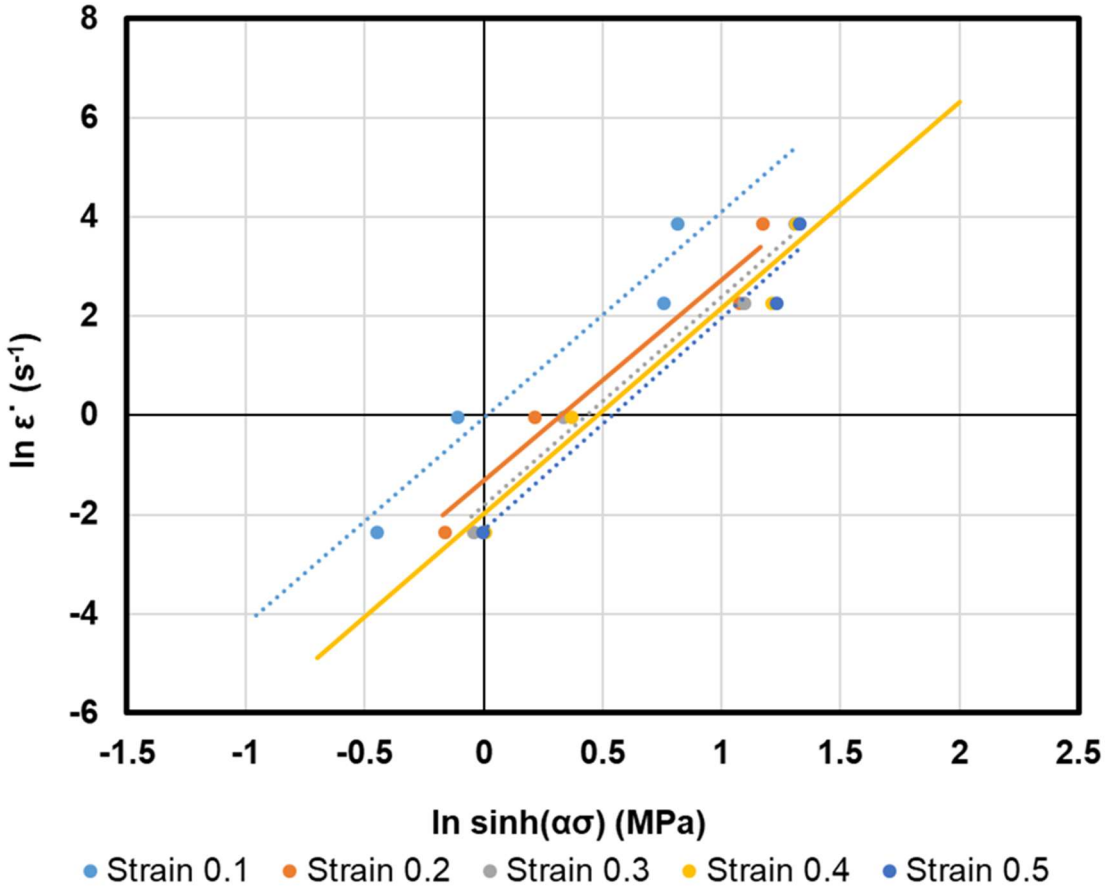

Temperature (°C)	850	850	850	850	850
Strain	0.5	0.4	0.3	0.2	0.1
n	4.2715	4.1448	4.2178	4.0456	4.1618
Y axis intercept	-2.295	-19864	-1.827	-1.31	-0.037
R^2	0.9657	0.9521	0.9754	0.9506	0.9384

c)

Figure 4 – Plots used for the determination of the material constants in VN steel a) $\boldsymbol{n'}$, b) $\boldsymbol{\beta}$ and c) $\boldsymbol{n}$ for Power law, Exponential law and Hyperbolic sinh law, respectively. The plots are for deformation at 750 °C and strain rates of 0.1, 1, 10 and 50 s^{-1}

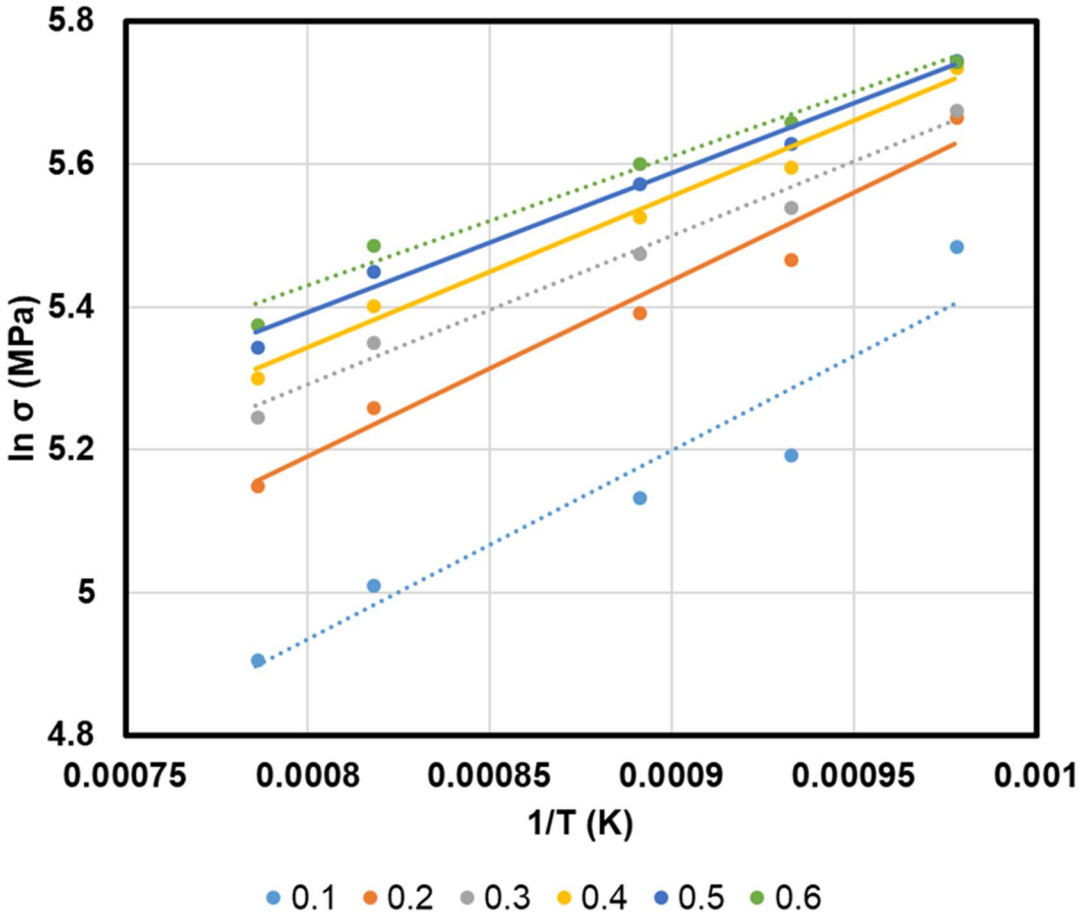

Strain rate (s^{-1})	10	10	10	10	10	10
Strain	0.6	0.5	0.4	0.3	0.2	0.1
Q/R	1808	1953	2112	2088.8	2457	2644.7
Y axis intercept	3.984	3.831	3.655	3.6202	3.226	2.8189
R^2	0.981	0.985	0.986	0.9852	0.969	0.9099

a)

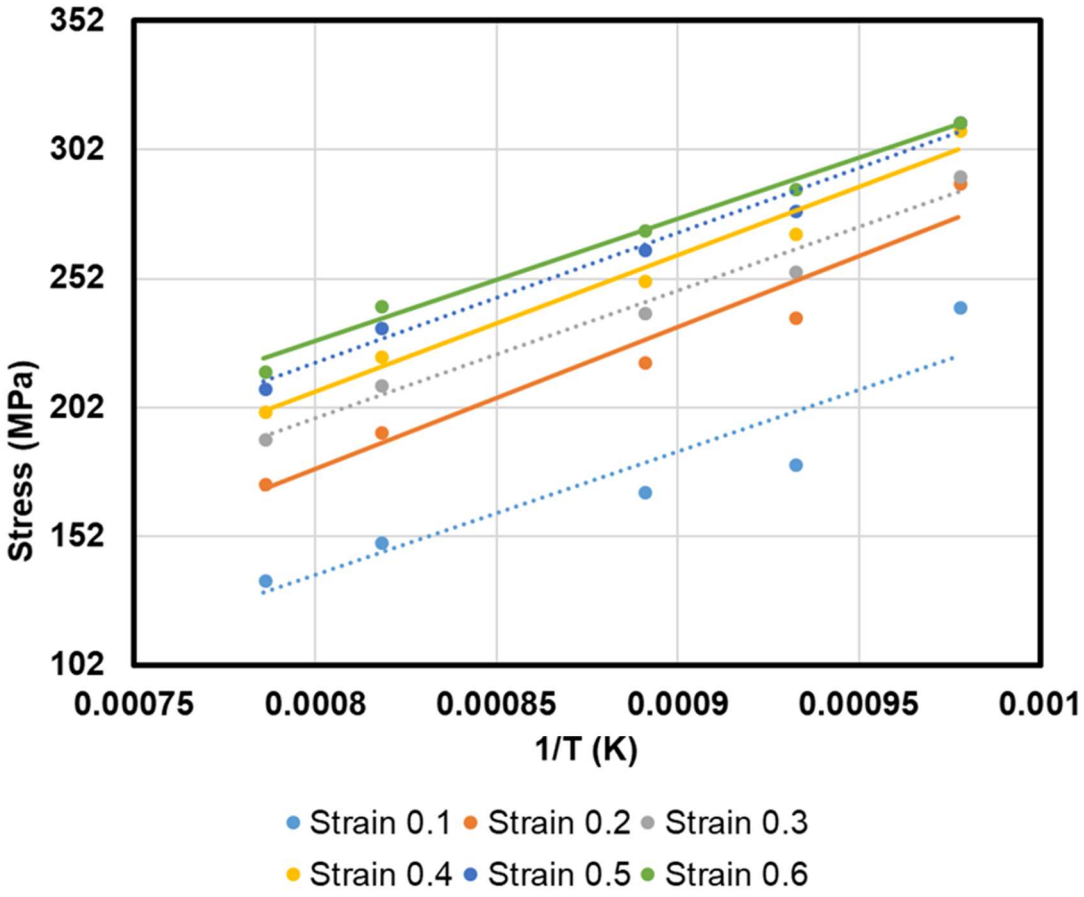

Strain rate (s^{-1})	10	10	10	10	10	10
Strain	0.6	0.5	0.4	0.3	0.2	0.1
Q/R	474263	503071	528438	494121	550138	477367
Y axis intercept	-151.5	-183.1	-214.3	-197.5	-261.9	-244.9
R^2	0.9886	0.9846	0.9763	0.9775	0.9427	0.8594

b)

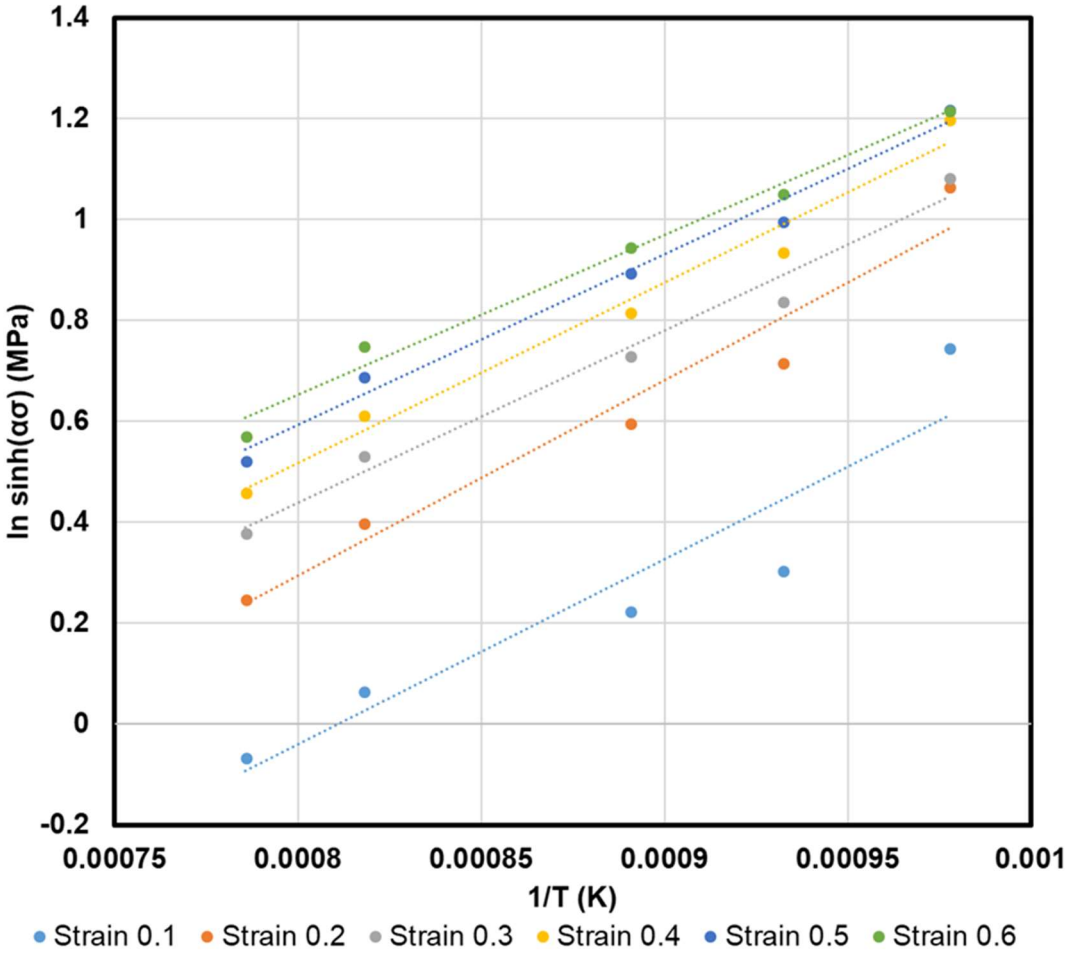

Strain rate (s^{-1})	10	10	10	10	10	10
Strain	0.6	0.5	0.4	0.3	0.2	0.1
Q/R	3173.2	3383	3583.4	3408	3868.3	3676.2
Y axis intercept	-1.886	-2.113	-2.35	-2.286	-2.8	-2.981
R^2	0.987	0.985	0.9797	0.981	0.9527	0.8849

c)

Figure 5 – Determination of the activation energy for hot working for the VN steel using the following kinetic relationships: a) Power law, b) Exponential law and c) Hyperbolic sinh law at a strain rate of 10 s^{-1}

3.3 Determination of characteristic and critical points

The critical strains, $\varepsilon_{c\,DT}$ and $\varepsilon_{c\,DRX}$, were determined by the inflections on the $\ln\theta$ versus ε plots. To distinguish $\varepsilon_{c\,DT}$ and $\varepsilon_{c\,DRX}$, the double differentiation technique was used where the critical strains were given by the minima in plots of dln θ/d$\boldsymbol{\varepsilon}$ vs $\boldsymbol{\varepsilon}$, see Figure 6 and tabulated in Table II for VN steel. The condition at $\varepsilon_{c\,DT}$ and $\varepsilon_{c\,DRX}$ in the $\ln\theta - \varepsilon$ curves were determined at a point when the second derivative of $\ln\theta$ with respect to ε becomes zero which can be expressed mathematically as [16]:

$$\frac{\partial^2 \ln\theta}{\partial\varepsilon^2} = 0 \qquad \text{Equation 7}$$

For flow curves that exhibited a peak, the critical points (critical strains and stresses) were expressed as a function of characteristic points (peak strain and peak stress) having the form: $\varepsilon_c = A\varepsilon_p$ or $\sigma_c = A'\sigma_p$ for both DT and DRX, a summary is given in Table III. For DT, the $\varepsilon_{c\,DT}$ was determined to be approximately $0.2\varepsilon_p$ for both VN and Nb-Ti steels.

Various workers have also reported that $\varepsilon_{c\,DRX}$ obeys a linear relationship with the Zener-Hollomon parameter, Z (i.e. $\varepsilon_c = AZ^q$) [32, 3]. Plots relating the peak and the Z parameter are given in Figure 7 and Figure 8 for strain and stress, respectively. A summary of the critical strains as a function of the Z parameter is given in Table IV. This dependence of the peak stress and strain on temperature and strain rate as expressed by Z, confirms that the deformation is controlled by a thermally activated process [32]. Table IV gives the expressions for the critical strains as a function of Z and the initial grain size, D_0.

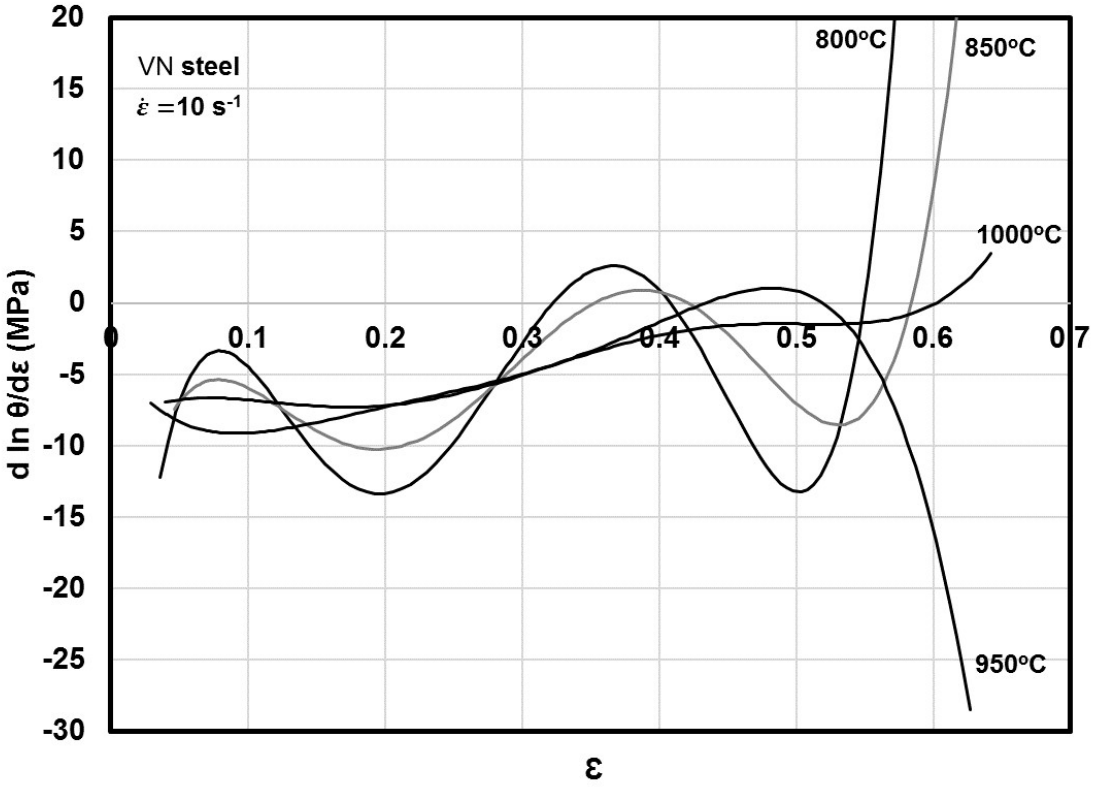

a)

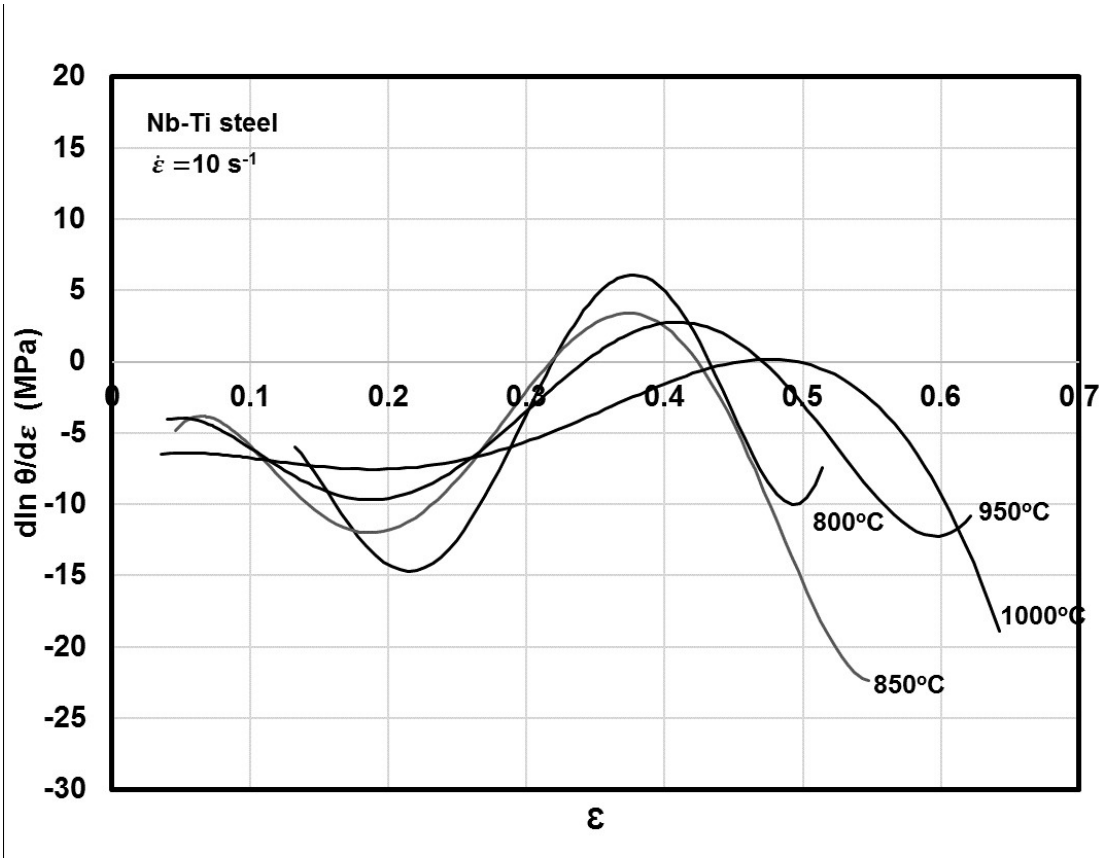

b)

Figure 6 – Plots of dln θ/d$\boldsymbol{\varepsilon}$ vs $\boldsymbol{\varepsilon}$ for a) VN steel and b) Nb-Ti steel at a strain rate of 10 s^{-1}

Table II – VN steel peak stress and strain obtained from $\boldsymbol{\sigma\theta - \sigma^2}$ plots (not shown here), and critical stress and strain obtained from Figure 6 at different temperatures and strain rates

Temperature (°C)	Strain rate, $\dot{\varepsilon}$ (s^{-1})	Peak stress (MPa)	Peak strain	Critical stress for DRX $\sigma_{c\ DRX}$ (MPa)	Critical strain for DRX $\varepsilon_{c\ DRX}$	Critical stress for DT $\sigma_{c\ DT}$ (MPa)	Critical strain for DT $\varepsilon_{c\ DT}$	Sat. stress σ_{sat} (MPa)
750	0.1	142.85	0.44	-	-	93	0.09	148.3
	1	187.4	0.4	181.62	0.28	129.3	0.11	202.5
	10	-	-	-	-	-	-	-
800	0.1	162.65	0.55	138.2	0.3	94	0.11	204.9
	1	177.6	0.44	-	-	120.6	0.12	189.7
	10			279.1	0.5	237.4	0.2	275.7
850	0.1	145.1	0.61	137.2	0.39	91.2	0.11	151.7
	1	158.9	0.52	-	-	105.4	0.11	165.8
	10			266.4	0.53	218.7	0.2	268.3
900	0.1	-	-	-	-	62.2	0.08	116.6
	1	148.2	0.57	-	-	100.2	0.11	151.7
	10	ND	ND	ND	ND	ND	ND	ND
950	0.1	-	-	80.6	0.34	55.1	0.12	95.9
	1	-	-	146.8	0.5	83.1	0.08	116.6
	10	-	-	-	-	143.7	0.1	245.0
1000	0.1	74.9	0.3	49.2	0.06	-	-	80.6
	1	-	-	125	0.46	85.7	0.09	130.4
	10	-	-	210.9	0.53	164	0.18	223.6

Table III – A summary of critical ratios for both strain and stress for dynamic transformation and recrystallization in the unstable austenite region

Steel type	$\varepsilon_{cDT}/\varepsilon_p = A_{DT}$	$\sigma_{cDT}/\sigma_p = A'_{DT}$	$\varepsilon_{cDRX}/\varepsilon_p = A_{DRX}$	$\sigma_{cDRX}/\sigma_p = A'_{DRX}$
VN steel	0.22	0.65	0.63	0.92
Nb-Ti steel	0.19	0.68	0.51	0.87
NOTE – In VN steel the standard deviation for both A_{DT} and A'_{DT} was 0.03. The standard deviation for A_{DRX} and A'_{DRX} was determined to be 0.08 and 0.06 respectively. In Nb-Ti steel the standard deviation for A_{DT} was 0.03 while for A'_{DT} was 0.1. The standard deviation for A_{DRX} and A'_{DRX} was determined to be 0.05 and 0.03 respectively.				

Table IV – Peak strain and stress relationship with the Zener-Hollomon parameter, Z

Steel type	$\varepsilon_p = AZ^q$	$\sigma_p = AZ^{q'}$
VN steel	$2.133Z^{-0.11}$ or $0.182D_0^{0.5}Z^{-0.11}$	$29.183Z^{0.124}$ or $2.484D_0^{0.5}Z^{0.124}$
Nb-Ti steel	$2.126Z^{-0.084}$ or $0.165D_0^{0.5}Z^{-0.084}$	$50.15Z^{0.070}$ or $3.89D_0^{0.5}Z^{0.070}$

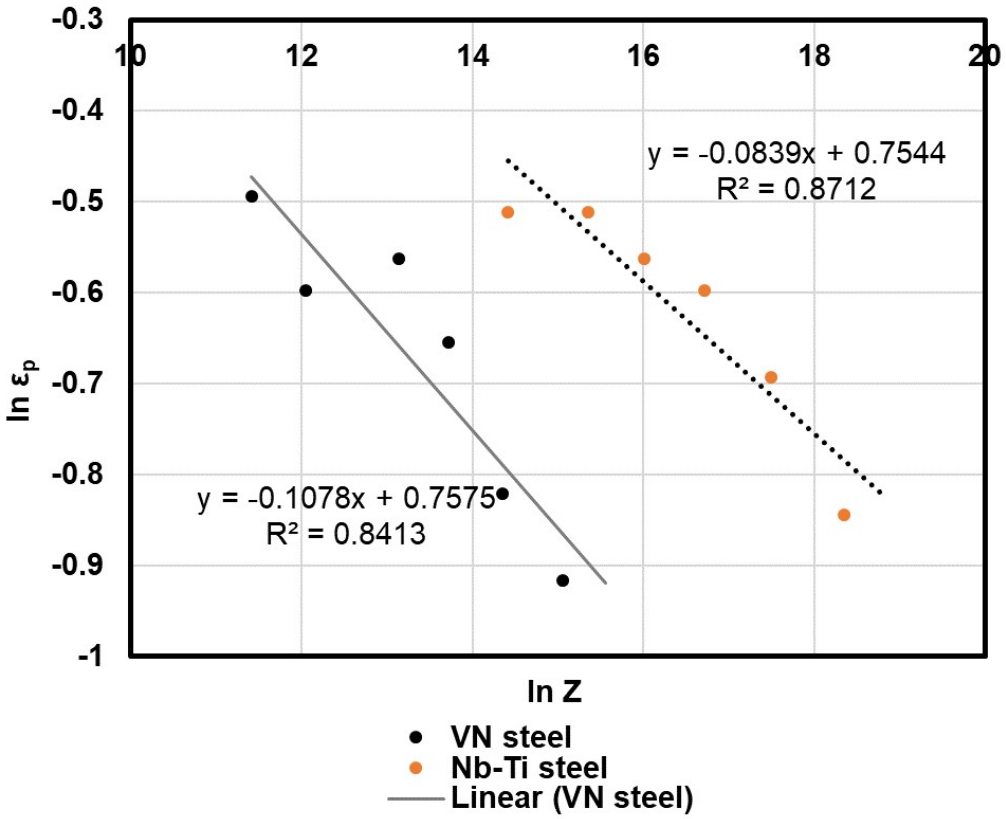

Figure 7 – Relationship between the peak strain and the Zener-Hollomon parameter for VN steel and Nb-Ti steel

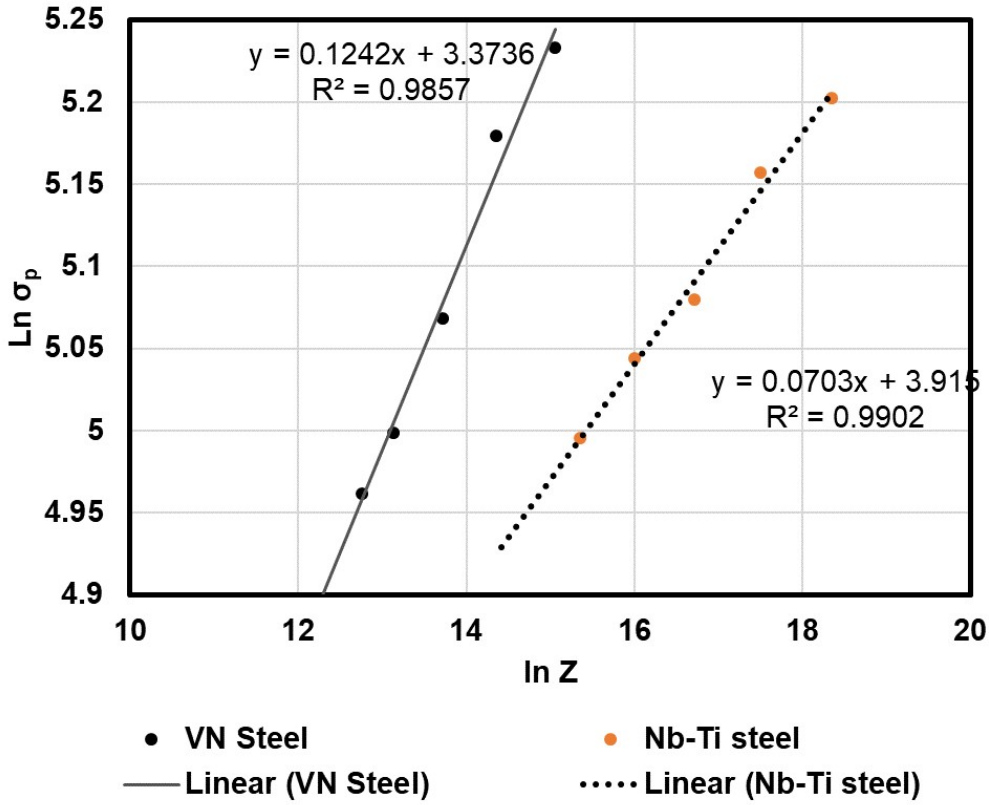

Figure 8 – Relationship between the peak stress and the Zener-Hollomon parameter for VN steel and Nb-Ti steel

3.4 Stress reduction due to DT and DRX

The approach proposed by Park et. al. [33] on the determination of softening due to dynamic transformation using the JMAK expression was used in this study, where stress reduction due to softening is given by:

$$\Delta\sigma = A\left\{1 - \exp\left[-B\left(\frac{\varepsilon-\varepsilon_c}{\varepsilon_p}\right)\right]\right\}^n \qquad \text{Equation 8}$$

where A, B and n are constants, ε_c is the critical strain and ε_p is the peak or maximum strain

The kinetic relationships for DT and DRX in the unstable austenite temperature region are given in Figure 12. The material constants were determined from various plots of $\ln\ln\Delta\sigma$ versus $\ln\left(\frac{\varepsilon-\varepsilon_c}{\varepsilon_p}\right)$ for n and $\ln\Delta\sigma$ against $\left(\frac{\varepsilon-\varepsilon_c}{\varepsilon_p}\right)$ for A and B, see Figure 9.

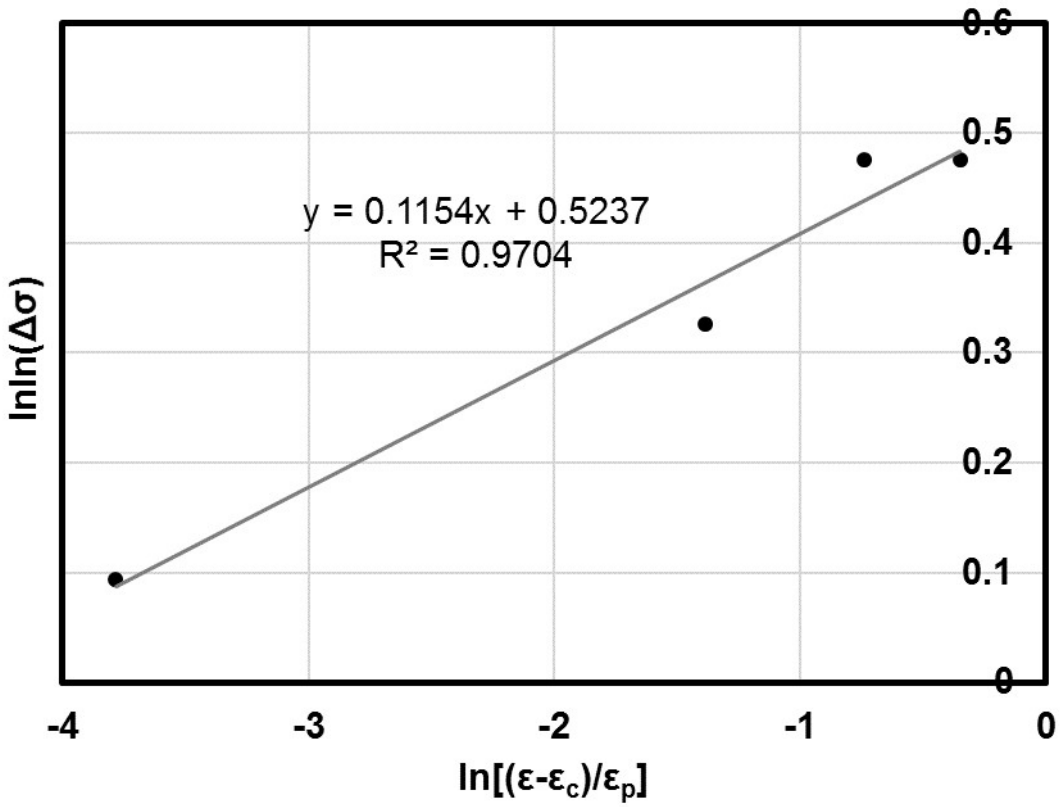

a)

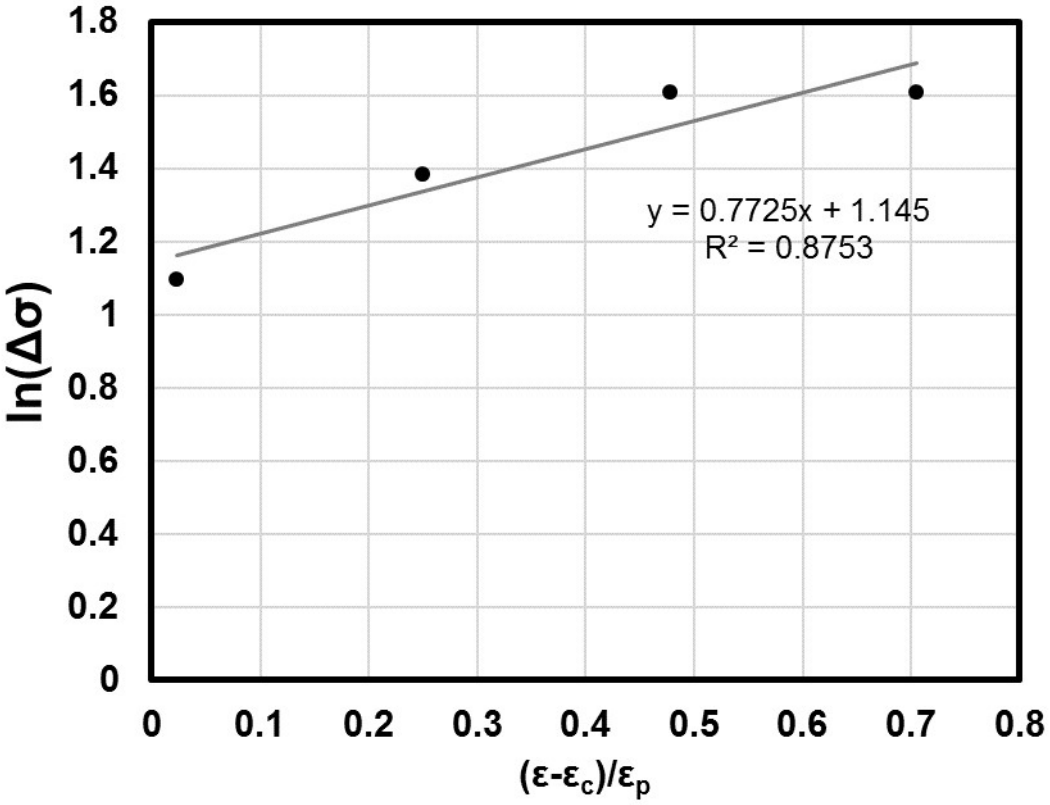

b)

Figure 9 – Plots for the determination of stress reduction constants due to dynamic transformation for the following a) n and b) B

3.5 Microstructure observations

Quantitative analysis of Prior Austenite Grain size (PAGS) is given in Chalimba et al. [35]. The mean prior austenite grains size for VN steel was lower than that of Nb-Ti steel i.e. 138 and 168 μm respectively. In studying the softening mechanisms, deformation was done at varying temperatures (750 to 1000 ^{o}C) and strain rates of 0.1, 1, 10 and 50 s^{-1}. In agreement with Aranas et al. [15], the transformation products were a ferritic microstructure with Widmanst*ä*tten ferrite observed where dynamic transformation was present, see Figure 10 a) and b). The displacively formed Widmanst*ä*tten ferrite then coalesced to form polygonal ferrite upon further straining or deformation in certain cases. Polygonal ferrite was also commonly observed at higher temperatures where dynamic recrystallization was dominant, see Figure 10 c). Comparatively, the grain sizes for Nb-Ti were slightly larger than those obtained in VN steels at temperatures lower than 1000^{o}C. This could be attributed to the fact that at lower temperatures DT was the only softening mechanism in VN steels while in Nb-Ti, DT was subsequently followed by DRX which could have also contributed to the variation in grain sizes for the Nb-Ti steels. At 1000^{o}C, DT was followed by DRX for both VN and Nb-Ti steels and the grain sizes were comparable at approximately 9 μm, see Figure 10 c) and f). In accordance with numerical results given in 3.3 above, dynamic transformation was present at higher temperatures above the Ar_3 with increase in strain rate typical to the rate of deformation experienced in finish rolling of strip steels.

The identification and quantification of DT and DRX grains was done using Electron Backscatter Scatter Diffraction (EBSD) method see Figure 11. The effect of increasing temperature and strain rate is summarized in Figure 12. At lower temperatures DT was the only softening mechanism while at intermediate temperatures both DT and DRX were present, see Figure 12 a). DRX was the only dominant softening mechanism. DT was present at higher temperatures with increasing strain rate. It should be noted that the step size of the EBSD images was large and ideal for grain size of approximately 10 μm. This study focused on MFS modelling and the EBSD images, therefore, only provided evidence of DT and DRX as the main softening mechanisms.

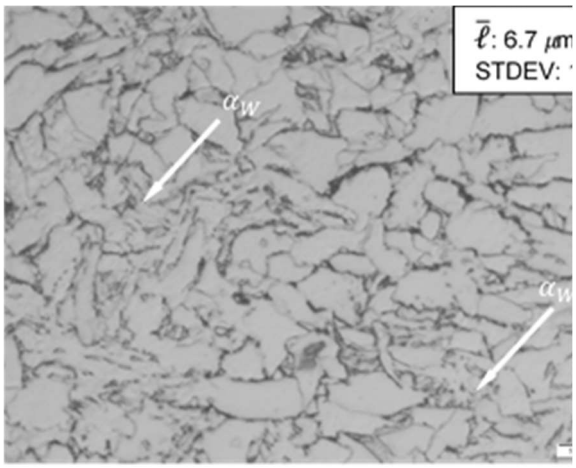

a)

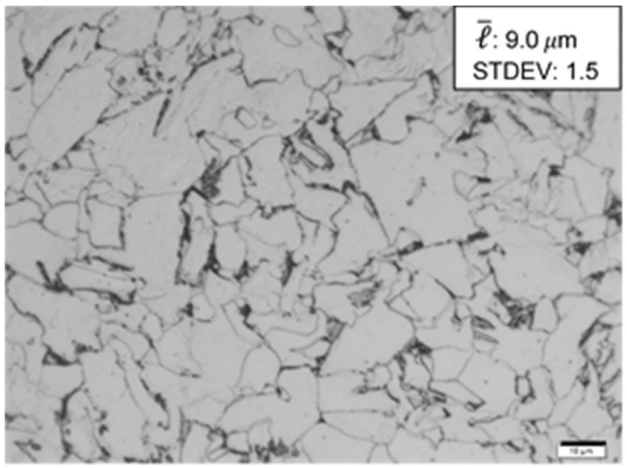

c)

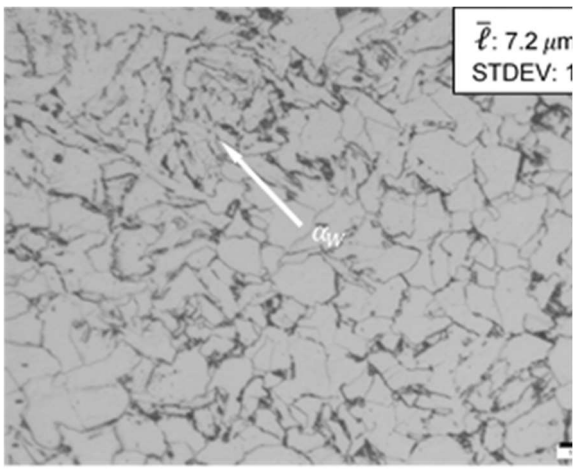

b)

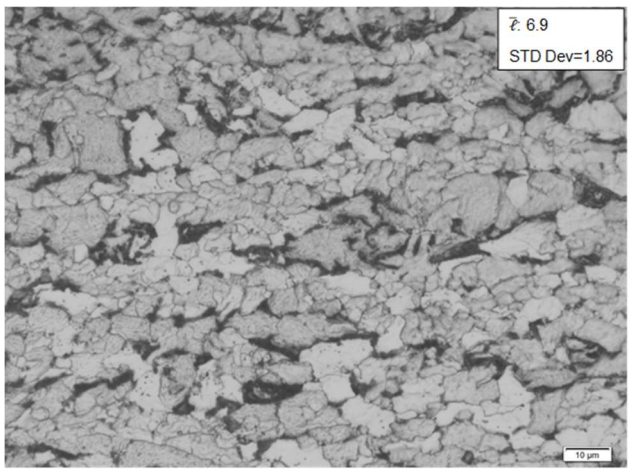

d)

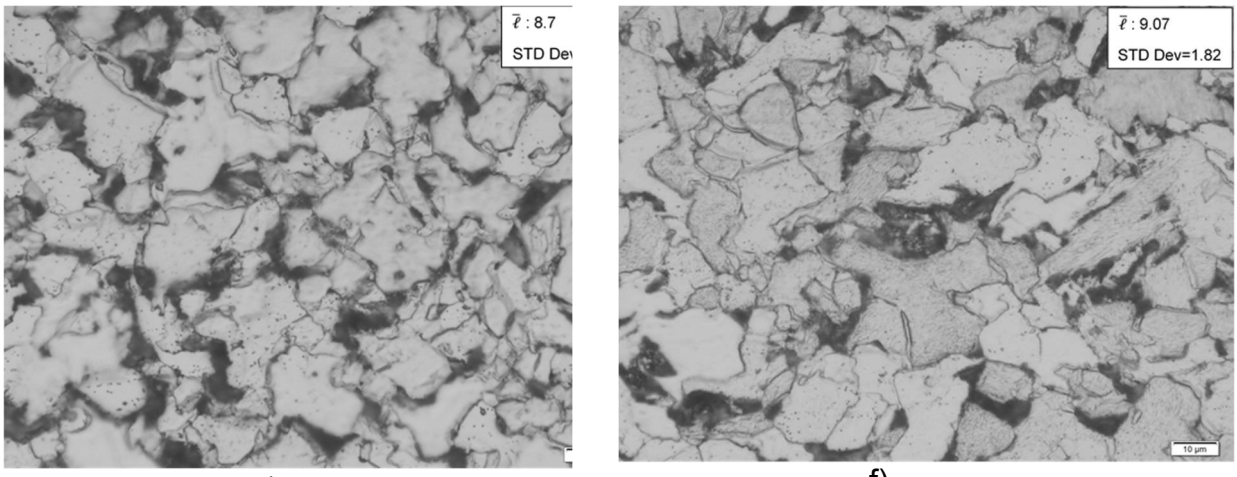

e) f)

Figure 10 – Optical micrographs with a scale bar of 10 μm and their respective mean intercept length ℓ, at strain rate of 0.1 s^{-1} and varying temperature a) 750°C, b) 900°C and c) 1000°C for VN steel, and d) 750°C, e) 900°C and f) 1000°C for Nb-Ti steel

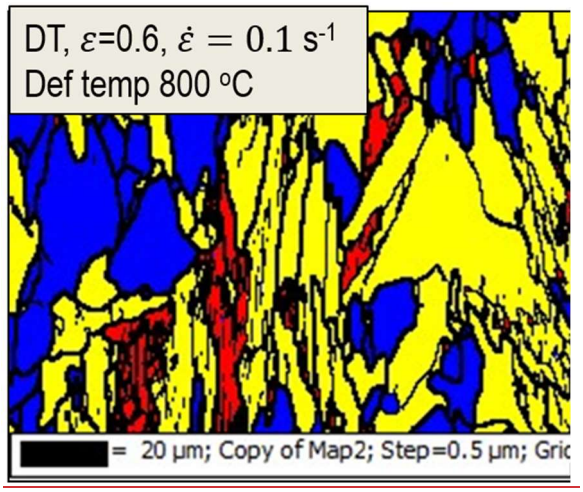

a) At $\dot{\varepsilon}$=0.1 and temperature 800°C

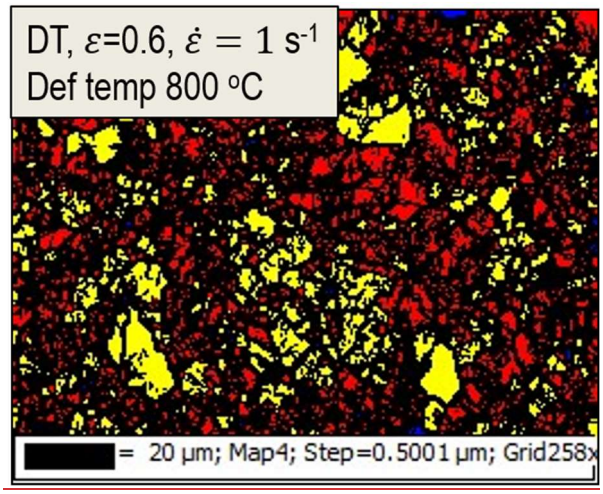

c) At $\dot{\varepsilon}$=1 and temperature 800°C

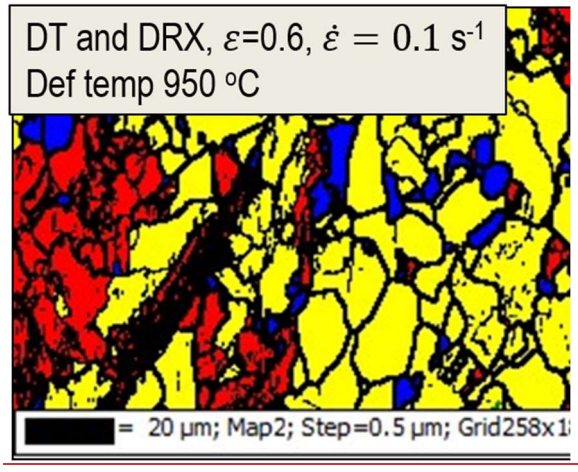

b) At $\dot{\varepsilon}$=0.1 and temperature 950°C

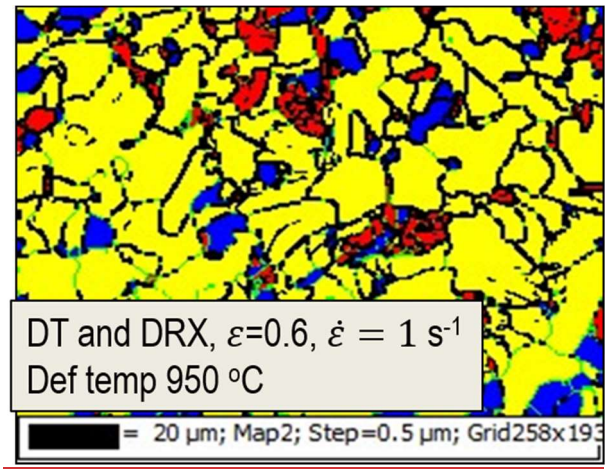

d) At $\dot{\varepsilon}$=1 and temperature 950°C

Figure 11 – EBSD images of VN steel strained to 0.6 with 7.5° as minimum misorientation angle to separate grains and 1° as minimum misorientation angle to separate subgrains, θ_c. Yellow represents substructured grains, red is for deformed grains and blue for recrystallized and/or dynamically transformed grains

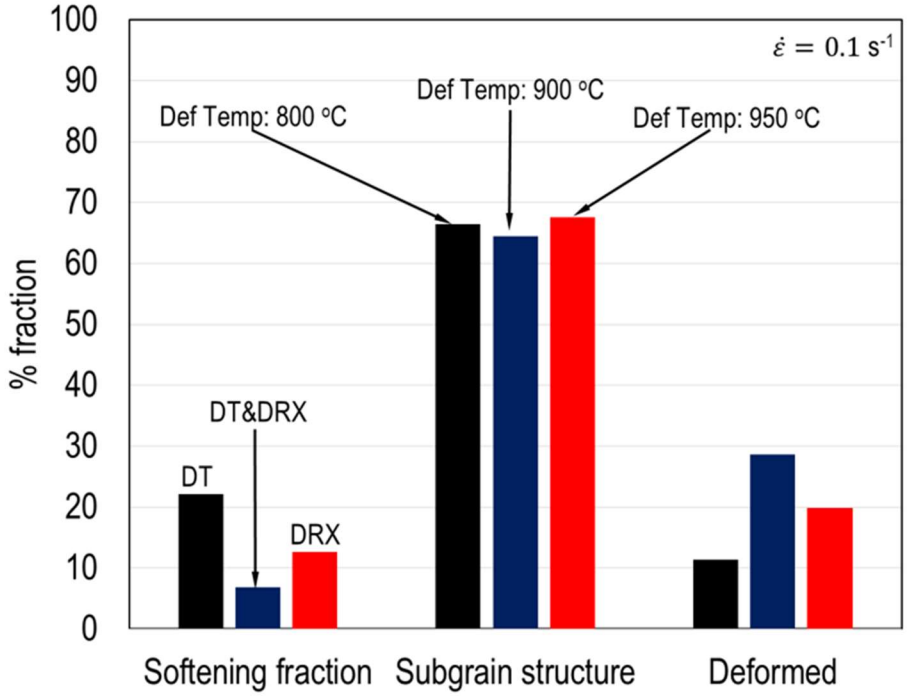

a)

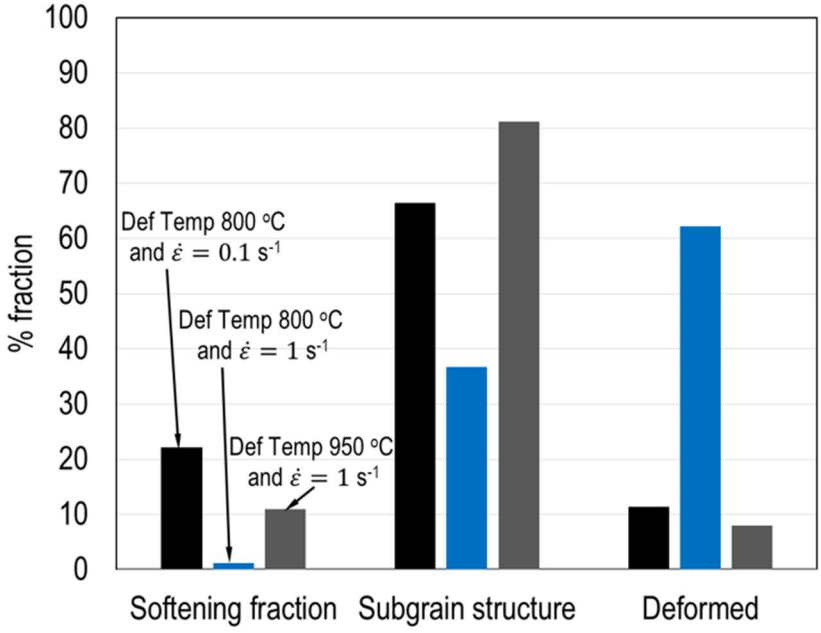

b)

Figure 12 – A summary of the effect of a) temperature and b) rate of deformation on softening mechanisms and their volume fractions

4.0 Discussion

4.1 Activation energy for hot working

In this investigation, the activation energy for hot working, Q_{HW}, is evaluated to be ~156 kJ/mol for the Nb-Ti and ~128 kJ/mol for the VN steels respectively, which are close to the dislocation core diffusion activation energy (159 kJ/mol) [21]. It should be noted that the Q_{HW} was found to be much lower than the self-diffusion activation energy in austenite 284 kJ/mol or ferrite 251 kJ/mol. However, the Q_{HW} reported in this study are comparable to those reported by Zhao et al. [21]. Using the Schöcks stress dependent model, Zhao et al. [21] working on medium Carbon Vanadium microalloyed steels, reported that the activation energy at different stress levels were in the range of 110.6–165.3 kJ/mol and identified dislocation slip to be the rate controlling mechanism at high strain rates which were comparable to those applied in this study. However, the challenge in using the Arrhenius equations in the unstable austenite region was the strain dependence of the material constants.

4.2 Critical points

The strain at which flow softening due to DT and DRX is initiated is of considerable industrial importance as the progression of both DT and DRX leads to decreases in the net work-hardening rate (i.e. rolling load in industrial processes) compared to expected values when DRV is the only restoration mechanism [22]. The critical stress for initiation of DRX ($\sigma_{c\,DRX}$) or DT ($\sigma_{c\,DT}$) may be determined by metallography, however, this approach is tedious requiring extensive sampling before and after the critical strain [19, 16, 23]. Furthermore, phase changes during cooling from the hot rolling temperature alter the deformed structure, which in turn render difficulties in precision of metallographic analysis [19, 16, 24]. Jonas and co-workers [3] proved it is also possible to determine both $\sigma_{c\,DT}$ and $\sigma_{c\,DRX}$ through the double differentiation technique. Furthermore, Poliak and Jonas also showed that the inflection in plots of $\ln\theta - \varepsilon$ and $\ln\theta - \ln\sigma$ curves may be used for the determination of critical strains $\varepsilon_{c\,DT}$ and $\varepsilon_{c\,DRX}$ [16, 19, 25, 26]. However, comparison between correlation coefficients indicates that the $\theta - \sigma$ curve analysis is more appropriate for the determination of σ_c while the $\ln\theta - \varepsilon$ curve analysis predicts the ε_c more accurately [16].

Consistent with work by other authors, the critical strain for dynamic transformation $\varepsilon_{c\,DT}$ preceded the critical strain for dynamic transformation $\varepsilon_{c\,DRX}$ where both mechanism were present. Both $\varepsilon_{c\,DT}$ and $\varepsilon_{c\,DRX}$ were lower than the peak strain, ε_p. Mostly the critical strain is expressed as a function peak strain, $\varepsilon_c = A\varepsilon_p$ or as the critical ratio, $R_c = \frac{\varepsilon_c}{\varepsilon_p}$ [25]. The ε_c and ε_p have a linear relationship and are reported to be dependent on temperature, strain rate and grain size [27]. Using the Poliak and Jonas approach, Ebrahimi and Solhjoo [23] reported the critical strain values for DRX to vary between $0.46\varepsilon_p$ to $0.55\varepsilon_p$ for different Nb microalloyed steel alloys which formerly were reported as $\varepsilon_{c\,DRX} = 0.8\varepsilon_p$ by microscopic observations. Most authors utilising the microscopic and other analytical techniques have reported values of the normalised critical stress for DRX to peak stress to be in the range of 0.6 to 0.8 for DRX [28, 3, 1, 29]. Stumpf [30] and Devadas [31] used an average critical ratio of 0.8 for various low

carbon strip steels. In this study, the $\varepsilon_{c\ DRX}$ was found to be approximately $0.63\varepsilon_p$ for VN steel and $0.51\varepsilon_p$ for Nb-Ti steel.

It can also be observed from Table II that DT has a weak thermal relationship supporting the propositions that DT is displacive in nature. It would also be suggested here that the weak temperature dependence could be that the mechanical deformation acts as an additional driving force which diminishes the required thermal component for the transformation. From the double differential plots, dynamic transformation was present at 117 ºC and 133 ± 25 ºC above the Ae_3 for VN steel and Nb-Ti steel, respectively. The presence of DT at high temperatures highlights the challenge in most flow stress models from the literature which overestimate flow stresses in low temperature work-hardened austenite as the softening effects of DT are neglected.

4.3 Stress reduction due to softening

The stress reduction due to both DT and DRX was expressed in form of a JMAK equation. The maximum strain considered in this study was the peak strain since σ_p or ε_p is not exceeded in most industrial hot strip near-finish rolling applications. It should also be noted that the use of the peak in the JMAK expression has been widely applied in the determination of recrystallized fraction X_{DRX}, in hot working by various workers including Fernandez et al. [34] and Momeni et al. [1]. However, at high temperatures which is not within the scope of this work, the JMAK relationship which utilises the maximum softening rate is frequently used. In the unstable austenite region, the work-hardening rate was monotonously reduced with strain and the maximum softening rate was indeterminate. This entails that softening in the inter-mode DRX/DT and DT regime is strain dependent and increases with strain rather than being time dependent. The softening kinetics, therefore, as reported in most studies may be expressed by a strain dependent JMAK expressions given in Table V.

The kinetic relationships given in Table V can be used independently or may be incorporated into existing flow stress models i.e. both empirical and physically-based models and FE codes currently in industrial use.

Table V – JMAK Stress drop expression for dynamic softening in VN and Nb-Ti steels

	VN steel	Nb-Ti steel
Stress reduction due to DT, $\Delta\sigma_{DT}$	$\Delta\sigma = 3.142\left\{1-\exp\left[-2.03\left(\frac{\varepsilon-\varepsilon_{c\ DT}}{\varepsilon_p}\right)\right]\right\}^{0.12}$	$\Delta\sigma = 9.85\left\{1-\exp\left[-17092\left(\frac{\varepsilon-\varepsilon_{c\ DT}}{\varepsilon_p}\right)\right]\right\}^{0.11}$
Stress reduction due to DRX, $\Delta\sigma_{DRX}$	$\Delta\sigma = 2.97\left\{1-\exp\left[-107.16\left(\frac{\varepsilon-\varepsilon_{c\ DRX}}{\varepsilon_p}\right)\right]\right\}^{0.07}$	$\Delta\sigma = 9.54\left\{1-\exp\left[-32080\left(\frac{\varepsilon-\varepsilon_{c\ DRX}}{\varepsilon_p}\right)\right]\right\}^{0.1}$

4.4 Flow stress up to its peak value

Research in hot working involves the determination of the dependency of stress on deformation parameters and is generally expressed in the form of kinetic rate equations [21]. In this investigation, the flow stress was modelled up to the peak and/or a maximum strain ε of 0.6. Under these conditions the kinetics of work-hardening, DRV, DT and DRX controlled the flow stress. The mathematical model presented below covers the effects of work-hardening and DRV mechanisms on the flow stress through the theoretical DRV work-hardening flow stress σ_{DRV}, see 3.1. The stress reduction due to softening mechanisms $\Delta\sigma_{DT}$ for stress reduction due to DT and $\Delta\sigma_{DRX}$ for reduction due to DRX, have also been considered, see 3.4.

When $\varepsilon \leq \varepsilon_{c\,DRX}$, the flow stress σ, is defined by the following relationship in the low temperature austenite region:

$$\sigma = \sigma_{DRV} - \Delta\sigma_{DT} \qquad \text{Equation 9}$$

When $\varepsilon > \varepsilon_{c\,DRX}$, the flow stress is defined by:

$$\sigma = \sigma_{DRV} - \Delta\sigma_{DT}{}' - \Delta\sigma_{DRX} \qquad \text{Equation 10}$$

Where $\Delta\sigma_{DT}{}'$ is the stress reduction due to DT at $\varepsilon = \varepsilon_{c\,DRX}$

The model given above is applicable up to the peak stress or to a strain of 0.6, whichever comes first. The effects of precipitation on the flow stress model have been accounted for in the work-hardening, however, softening due to nucleation of precipitates has not been addressed in this model. The model does not cover any static changes/effects which may be incorporated in microstructural evolution models.

In general, the model presented above gives better Mean Flow Stress (MFS) predictions for both VN and Nb-Ti steels, and is applicable in the unstable austenite temperature region, Figure 13. Better correlation between the predicted flow stress and measured values was attained, see Figure 14.

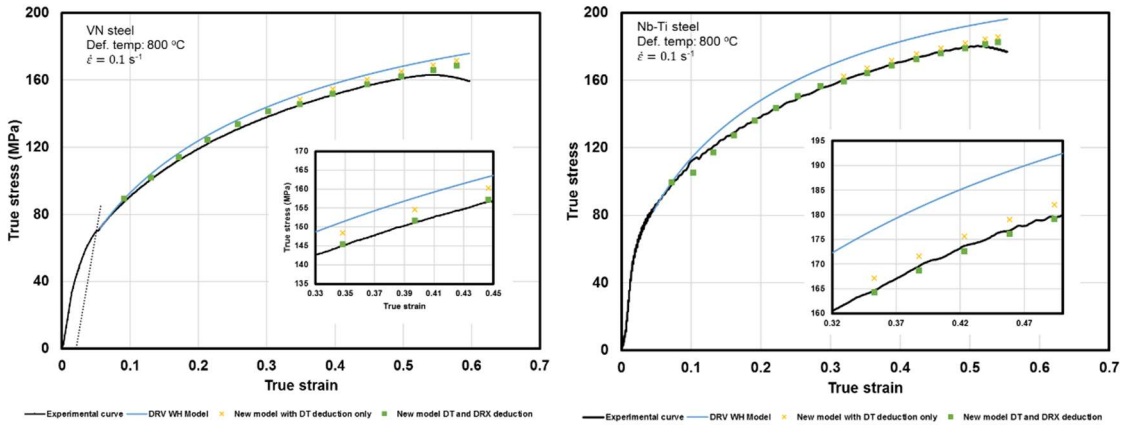

Figure 13 – Comparison between the experimental flow curve and the predicted flow curve for a) the VN steel and b) the Nb-Ti steel

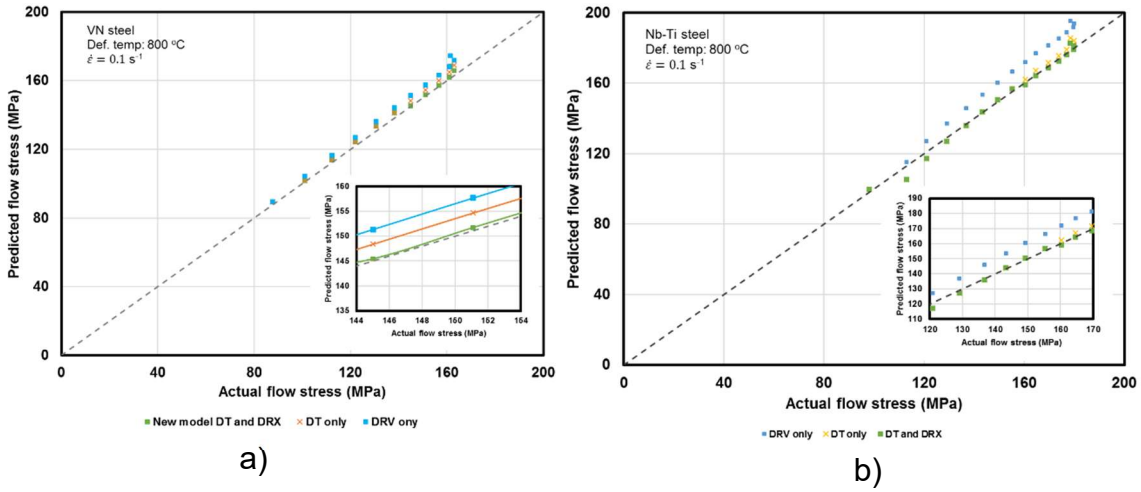

Figure 14 – Predicted flow stress versus the actual flow stress for a) the VN steel and b) the Nb-Ti steel

5.0 Conclusions

1) A constitutive flow stress model is proposed which estimates the hot working flow curve up to its peak or a strain of 0.6. The model incorporates the effects of dynamic recrystallization and dynamic transformation and, therefore, extends into the lower temperature unstable austenite area of finish hot strip rolling. The model attained good predictive capabilities. The model is restricted, however, to dynamic hot working behaviour and any contributions from the static behaviour will have to be covered by microstructural evolution models.

2) A modified expression for the determination of a DRV-only curve in the unstable austenite temperature region has been used.

3) Expressions for softening kinetics for both dynamic transformation (DT) and dynamic recrystallization (DRX) have been presented.

4) The Hot deformation activation energy determined was found to be 128 kJ/mol for the VN steel and 156 kJ/mol for the Nb-Ti steel which is in good agreement with values obtained from activation volume methods and suggesting cross slip to be the active mechanism.

5) The model should allow improved predictions of the Mean Flow Stress and thereby also of mill loads for the finishing passes of hot strip rolling of both VN and Nb-Ti microalloyed steels.

Acknowledgements
This work has been performed with funding from the University of Pretoria and technical support from the Industrial Minerals and Metals Research Institute (IMMRI). Generous help from Rorisang Maubane is gratefully acknowledged for

providing on-equipment training and technical support on the Bähr 850AD™ and Gleeble 1500™ during tests. Work on Gleeble™ 3500 was done at the University of Cape Town with support from Sara George. Support on microscopy from Carel Cotzee is greatly acknowledged.

References

[1] A. Momeni, S. M. Abbasi and H. Badri, “Hot deformation bahaviour and constitutive modelling of VCN 200 low alloy steel,” *Applied Mathematical Modelling,* vol. 36, pp. 5624-5632, 2012.

[2] M. Meysami and S. A. A. A. Mousavi, “Study on behaviour of medium carbon vanadium microalloyed steel by hot compression test,” *Materials Science and Engineering A,* vol. 528, pp. 3049-3055, 2011.

[3] H.-l. Wei, G.-q. Liu, X. Xiao and M.-h. Zhang, “Dynamic recrystallization behavior of a medium carbon vanadium microalloyed steel,” *Materials Science and Engineering A,* vol. 573, pp. 215-221, 2013.

[4] A. A. Gorni, *Steel Forming and Heat Treating Handbook,* São Vicente SP, Brazil: www.gorni.eng.br, 2015.

[5] S. Shida, “Empirical formula of flow stress of carbon steels - resistance to deformation of carbon steels at elevated temperature,” *Journal of Japan Society for Technology of PLasticity,* vol. 10, pp. 610-617, 1969.

[6] S. A. J. Chalimba, R. J. Mostert, W. E. Stumpf, K. M. Banks and C. W. Siyasiya, “Modelling of Work-Hardening during Hot Rolling of V and Nb Microalloyed Steels in the Low Austenite Temperature Region,” *Journal of Materials Engineering and Performance,* vol. 26, no. 11, pp. 5217-5227, 2017.

[7] B. Roebuck, J. D. Lord, M. Brooks, M. S. Loveday, C. M. Sellars and R. W. Evans, Measurement Good Practice Guide No 3 - Measuring Flow Stress in Hot Axisymmetric Compression Tests, United Kingdom: National Physical Laboratory, 2002.

[8] C. Devadas, D. Baragar, G. Ruddle and I. V. Samarasekera, “The Thermal and Metallurgical State of Steel of Steel Strip during Hot Rolling: Part II. Factors Influencing Rolling Loads,” *Metallurgical Transactions A,* vol. 22A, pp. 321-333, 1991.

[9] Dynamic Systems Inc, Gleeble Systems Application Note: Flow Stress Correction in Uniaxial Compression Testing, New York: DSI, 2003.

[10] S. A. J. Chalimba, R. J. Mostert, W. Stumpf, K. M. Banks and C. W. Siyasiya, “Effects of roughing on finish rolling simulations in microalloyed strip steels,” *Accepted for publication,* 2016.

[11] C. Ghosh, “The Dynamic Transformation of Deformed Austenite at Temperatures above the Ae3,” PHd Thesis, McGill University, Montreal, Canada, 2013.

[12] J. J. Jonas, X. Quelennec, L. Jiang and E. Martin, “The Avrami kinetics of dynamic recrystallization,” *Acta Materialia,* vol. 57, pp. 2748-2756, 2009.

[13] E. I. Poliak and J. J. Jonas, “A one-parameter approach to determining the critical conditions for the initiation of dynamic recrystallization,” *Acta mater.,* vol. 44, no. 1, pp. 127-136, 1996.

[14] J. J. Jonas, C. Ghosh, X. Quelennec and V. V. Basabe, “The Critical Strain for Dynamic Transformation in Hot Deformed Austenite,” *ISIJ International,* vol. 53, no. 1, pp. 145-151, 2013.

[15] C. J. Aranas, R. Grewal, K. Chadha, D. Shahriari, M. Jahazi and J. J. Jonas, “Formation of widmanstatten ferrite in a C-Mn steel at temperatures high in the austenite phase field,” in *Proceedings of the International Conference on Solid-Solid Phase Transformations in Inorganic Materials 2015*, 2015.

[16] H. Mirzadeh and A. Najafizadeh, “Prediction of the critical condition for initiation of Dynamic Recrystallization,” *Materials Design,* vol. 31, pp. 1174-1179, 2010.

[17] Y. Estrin and H. Mecking, “A unified phenomenological description of work hardening and creep based on one-parameter models,” *Acta Metall.,* vol. 32, no. 1, pp. 57-70, 1984.

[18] A. Cingara and H. J. McQueen, “New method for determining sinh constitutive constants for high temperature deformation of 300 austenitic steels,” *Journal of Materials Processing Technology,* vol. 36, pp. 17-30, 1992.

[19] R. Ebrahimi and E. Shafiei, “Mathematical Modeling of Single Peak Dynamic Recrystallization Flow stress curves in Metallic alloys,” 2012. [Online]. Available: http://www.intechopen.com/books/recystallization/mathematical-modelling-of-sinlge-peak-dynamic-recrystallization-flow-stress-curves-in-metallic-alloys. [Accessed 30 May 2015].

[20] C. M. Sellars and W. J. McTegart, “On the mechanism of hot deformation,” *Acta Metallurgica,* vol. 14, pp. 1136-1138, 1966.

[21] H. Zhao, G. Liu and L. Xu, “Rate controlling mechanisms of hot deformation in medium carbon Vanadium microalloy steel,” *Material Science and Engineering A,* vol. 559, pp. 263-267, 2013.

[22] C. Ghosh, V. V. Basabe and J. J. Jonas, “Determination of the Critical Strains for the Initiation of Dynamic Transformation and Dynamic Recrystallization in Four Steels of Increasing Carbon Contents,” *Steel Research International,* vol. 84, no. 5, pp. 490-494, 2013.

[23] R. Ebrahimi and S. Solhjoo, “Characteristic Points of Stress-Strain Curve at High Temperature,” *International Journal of ISSI,* vol. 4, no. 1,2, pp. 24-27, 2007.

[24] T. Sakai, A. Belyakov, R. Kaibyshev, H. Miura and J. J. Jonas, “Dynamic and post-dynamic recrystallization under hot, cold and severe plastic deformation conditions,” *Progress in Materials Science,* vol. 60, pp. 130-207, 2014.

[25] R. C. K. Nkhoma, C. W. Siyasiya and W. E. Stumpf, “Hot working characteristics of AISI 321 in comparison to AISI 304 Austenitic stainless steels,” University of Pretoria, RSA, 2014.

[26] E. I. Poliak and J. J. Jonas, “Critical Strain for Dynamic Recrystallization in Variable Strain Rate Hot Deformation,” *ISIJ Intenational,* vol. 43, no. 5, pp. 692-700, 2003.

[27] P. Pauskar and R. Shivpuri, “Microstructure and Mechanics interaction in the Modeling of hot rolling of rods,” *Annals of the CIRP,* vol. 48/1/1999, pp. 191-194, 1999.

[28] H. Mirzadeh, J. M. Cabrera, J. M. Prado and A. Najafizadeh, “Hot deformation behaviour of a medium carbon microalloyed steel,” *Materials Science and Engineering A,* vol. 528, pp. 3876-3882, 2011.

[29] S. I. Kim and Y. C. Yoo, “Prediction of dynamic recrystallization behaviour of AISI type 4140 medium carbon steel,” *Materials Science and Technology,* vol. 18, pp. 160- 164, 2002.

[30] W. Stumpf, “Grain size modelling of a low carbon strip steel during hot rolling in a Compact Strip Production (CSP) plant using the Hot Charge Route,” *The Journal of The South African Institute of Mining and Metallurgy,* pp. 617-632, 2003.

[31] C. Devadas, “The prediction of the evolution of microstructure during hot rolling of steel strips,” PHD Thesis, University of British Columbia, United Kingdom, 1989.

[32] M. Shaban and B. Eghbali, “Determination of critical conditions for dynamic recrystallization of a microalloyed steel,” *Materials Science and Engineering A,* vol. 527, pp. 4320-4325, 2010.

[33] N. Park, S. Khamsuk, A. Shibata and N. Tsuji, “Effect of austenite grain size on kinetics of dynamic ferrite transformation in low carbon steel,” *Scripta Materialia,* vol. 68, pp. 611-614, 2013.

[34] A. I. Fernandez, P. Uranga, B. Lopez and J. M. Rodriguez-Ibabe, “Dynamic recrystallization behaviour covering a wide austenite grain size range in Nb and Nb-Ti microalloyed steels,” *Materials Science and Engineering A,* vol. 361, pp. 367-376, 2003.

[35] S. A. J. Chalimba, R. J. Mostert, W. Stumpf, K. M. Banks and C. W. Siyasiya, “Effects of Roughing on Finish Rolling Simulations in Microalloyed Strip Steels,” *Journal of Materials Engineering and Performance,* vol. 26, no. 11, pp. 5294-5303, 2017.

[36] S. H. Zahiri, S. M. Byon, S. Kim, Y. Lee and P. D. Hodgson, “Static and metadynamic recrystallization of Interstitial Free steels during hot deformation,” *ISIJ International,* vol. 44, no. 11, pp. 1918-1923, 2004.

[37] B. Eghbali, “Effect of strain rate on the microstructural development through continuous dynamic recrystallization in a microalloyed steel,” *Materials Science and Engineering A,* vol. 527, pp. 3402-3406, 2010.

[38] P. D. Hodgson, J. J. Jonas and C. H. J. Davies, “Modeling of hot and warm working of steels,” in *Handbook of thermal process modeling of steels Thermal Process Modelling of Steels*, New York, CRC Press, 2008, pp. 225-65.